

# Application of spectral phase shaping to high resolution CARS spectroscopy

S. Postma\*, A. C. W. van Rhijn, J. P. Korterik, P. Gross†, J. L. Herek,  
and H. L. Offerhaus

*Optical Sciences Group, Department of Science and Technology, MESA<sup>+</sup> Institute for Nanotechnology,  
University of Twente, 7500 AE Enschede, The Netherlands*

*† Current address: Optische Technologien, Institut für Angewandte Physik, Westfälische Wilhelms-Universität,  
D-48149 Münster, Germany*

\* Corresponding author: [s.postma@utwente.nl](mailto:s.postma@utwente.nl)  
<http://os.tnw.utwente.nl/>

**Abstract:** By spectral phase shaping of both the pump and probe pulses in coherent anti-Stokes Raman scattering (CARS) spectroscopy we demonstrate the extraction of the frequencies, bandwidths and relative cross sections of vibrational lines. We employ a tunable broadband Ti:Sapphire laser synchronized to a ps-Nd:YVO mode locked laser. A high resolution spectral phase shaper allows for spectroscopy with a precision better than  $1 \text{ cm}^{-1}$  in the high frequency region around  $3000 \text{ cm}^{-1}$ . We also demonstrate how new spectral phase shaping strategies can amplify the resonant features of isolated vibrations to such an extent that spectroscopy and microscopy can be done at high resolution, on the integrated spectral response without the need for a spectrograph.

©2008 Optical Society of America

**OCIS codes:** (190.7110) Ultrafast nonlinear optics; (300.6230) Spectroscopy; coherent anti-Stokes Raman scattering; (320.5540) Pulse shaping; (320.7150) Ultrafast spectroscopy

---

## References and links

1. P. D. Maker and R. W. Terhune, "Study of Optical Effects due to an induced Polarization Third Order in the electric field strength," *Phys. Rev.* **137**, A801-A818 (1965).
2. A. Zumbusch, G. R. Holtom, and X. S. Xie, "Three-dimensional vibrational imaging by Coherent Anti-Stokes Raman Scattering," *Phys. Rev. Lett.* **82**, 4142-4145 (1999).
3. M. D. Duncan, J. Reintjes, and T. J. Manuccia, "Scanning coherent anti-Stokes Raman microscope," *Opt. Lett.* **7**, 350-352 (1982).
4. J. Cheng, A. Volkmer, and X. S. Xie, "Theoretical and experimental characterization of coherent anti-Stokes Raman scattering microscopy," *J. Opt. Soc. Am. B* **19**, 1363-1375 (2002).
5. E. O. Potma, C. L. Evans, and X. S. Xie, "Heterodyne Coherent Anti-Stokes Raman Scattering (CARS) Imaging," *Opt. Lett.* **31**, 241-243 (2006).
6. M. Hashimoto, T. Araki, and S. Kawata, "Molecular vibration imaging in the fingerprint region by use of coherent anti-Stokes Raman scattering microscopy with a collinear configuration," *Opt. Lett.* **25**, 1768-1770 (2000).
7. M. Müller and J. M. Schins, "Imaging the Thermodynamic State of Lipid Membranes with Multiplex CARS Microscopy," *J. Phys. Chem B.* **106**, 3715-3723 (2002).
8. B. von Vacano, L. Meyer, and M. Motzkus, "Rapid Polymer blend imaging with quantitative broadband multiplex CARS microscopy," *J. Raman Spectrosc.* **38**, 916-926 (2007).
9. T. W. Kee and M. T. Cicerone, "Simple approach to one-laser, broadband coherent anti-Stokes Raman scattering microscopy," *Opt. Lett.* **29**, 2701-2703 (2004).
10. M. Okuno, H. Kano, P. Leproux, V. Couderc, and H. Hamaguchi, "Ultrabroadband ( $>2000 \text{ cm}^{-1}$ ) multiplex coherent anti-Stokes Raman scattering spectroscopy using a subnanosecond supercontinuum light source," *Opt. Lett.* **32**, 3050-3052 (2007).
11. S. Zhang, L. Zhang, X. Zhang, L. Ding, G. Chen, Z. Sun, and Z. Wang, "Selective excitation of CARS by adaptive pulse shaping based on genetic algorithm," *Chem. Phys. Lett.* **433**, 416-421 (2007).
12. J. Konradi, A. K. Singh, A. V. Scaria, and A. Materny, "Selective spectral filtering of molecular modes of  $\beta$ -carotene in solution using optimal control in four-wave-mixing spectroscopy," *J. Raman Spectrosc.* **37**, 697-704 (2006).
13. J. Konradi, A. Scaria, V. Nambodiri, and A. Materny, "Application of feedback-controlled pulse shaping for control of CARS spectra: The role of phase and amplitude modulation," *J. Raman Spectrosc.* **38**, 1006-1021 (2007).

14. N. Dudovich, D. Oron, and Y. Silberberg, "Single-pulse coherently controlled nonlinear Raman spectroscopy and microscopy," *Nature*, **418**, 512-514 (2002).
15. D. Oron, N. Dudovich, and Y. Silberberg, "Femtosecond Phase-and-Polarization Control for Background-Free Coherent Anti-Stokes Raman Spectroscopy," *Phys. Rev. Lett.* **90**, 213902-4 (2003).
16. T. Polack, D. Oron, and Y. Silberberg, "Control and measurement of a non-resonant Raman wavepacket using a single ultrashort pulse," *Chem. Phys.* **318**, 163-169 (2005).
17. A. M. Weiner, D. E. Leaird, G. P. Wiederrecht, and K. A. Nelson, "Femtosecond multiple-pulse impulsive stimulated Raman scattering spectroscopy," *J. Opt. Soc. Am. B* **8**, 1264-1275 (1991).
18. S. Lim, A. G. Caster, and S. R. Leone, "Single-pulse phase-control interferometric coherent anti-Stokes Raman scattering spectroscopy," *Phys. Rev A* **72**, 0418303-4 (2005).
19. H.-S. Tang and W. S. Warren, "Mid infrared pulse shaping by optical parametric amplification and its application to optical free induction decay measurement," *Opt. Express* **11**, 1021-1028 (2003).
20. D. Oron, N. Dudovich, and Y. Silberberg, "All-optical processing in coherent nonlinear spectroscopy," *Phys. Rev. A* **70**, 023415 (2004).
21. S. Postma, P. van der Walle, H. L. Offerhaus, N. F. van Hulst, "Compact high-resolution spectral phase shaper," *Rev. Sci. Instrum.* **76**, 123105-4 (2005).
22. T. Baumert, T. Brixner, V. Seyfried, M. Strehle, and G. Gerber, "Femtosecond pulse shaping by an evolutionary algorithm with feedback," *Appl. Phys. B*, **65**, 779-782 (1997).
23. L. Ma, R. K. Shelton, H. C. Kapteyn, M. M. Murnane, and J. Ye, "Sub-10-femtosecond active synchronization of two passively mode-locked Ti:sapphire oscillators," *Phys. Rev. A*, **64**, 021802-4 (2001).
24. R. W. Boyd, *Nonlinear Optics*, second edition (Academic Press, 2003), Chap. 10. "Stimulated Raman Scattering and Stimulated Rayleigh-Wing Scattering,"
25. J. Workman Jr., *Handbook of Organic Compounds: NIR, IR, Raman and UV-Vis Spectra featuring Polymers and Surfaces*, (Academic Press 2001), Vol. 3 IR and Raman Spectra.

## 1. Introduction

Coherent anti-Stokes Raman scattering (CARS) has been successfully used in spectroscopy and microscopy since the development of (tunable) pulsed laser sources [1-3]. In CARS, molecular vibrations are excited coherently by the pump ( $\omega_p$ ) and Stokes ( $\omega_s$ ) pulses. Subsequently a probe ( $\omega_{pr}$ ) pulse, which is often derived from the same pulse as the pump, generates the anti-Stokes signal ( $\omega_c = \omega_p - \omega_s + \omega_{pr}$ ). The energy diagram for a narrowband resonant CARS process is given in Fig. 1(a). Several schemes for broadband resonant CARS processes are visualized in Figs. 1(b)-1(d). The resonant CARS signal is accompanied by an inherent non-resonant background. The energy diagram for such a non-resonant process is depicted in Fig. 1(e).

When all the light pulses have a relatively small bandwidth (few  $\text{cm}^{-1}$ ) a CARS spectrum can be measured by tuning the difference frequency of ( $\omega_p - \omega_s$ ) [4-6]. A more direct way to obtain a CARS spectrum is multiplex CARS shown in Fig. 1(b), with a broadband ( $\sim 500 \text{ cm}^{-1}$ ) Stokes pulse. In this method the CARS signal is measured on a spectrometer [7-10]. Single pulse CARS, where  $\omega_p$ ,  $\omega_s$ , and  $\omega_{pr}$  are all part of the same broadband pulse, has also been investigated in conjunction with spectral phase and amplitude shaping. These experiments mainly employ broadband pump and Stokes pulses, in combination with a relatively narrow probe pulse as in Fig. 1(c). Due to interference between the shaped pump and Stokes pulses it is possible to enhance one transition and suppress other transitions [11-13]. With various phase and/or amplitude profiles of the pump and Stokes pulses vibrational frequencies and bandwidths are retrieved [14-18]. In practice, this technique reaches only vibrational frequencies below  $1500 \text{ cm}^{-1}$ .

Instead of broadband pump and Stokes pulses, we employ broad pump and *probe* pulses in combination with a narrow Stokes pulse as in Fig. 1(d). Since the Stokes pulse comes from an independent source we can set the center frequency difference to correspond to higher vibrational frequencies ( $\sim 3000 \text{ cm}^{-1}$ ). The narrow Stokes pulse ( $\sim 1 \text{ cm}^{-1}$ ) allows for direct projection of the phase profiles onto the molecule; the narrow Stokes essentially shifts the shaped pump profile to the vibrational frequencies without changing it. The phase profile that is programmed on the spectral phase shaper directly addresses the molecular profile just as it would in IR spectroscopy if the difference frequency generation was done separately (see e.g. [19]) but without the absorption and large focal size associated with IR wavelengths. Since the spatial phase modulator covers a range of frequencies in an almost linear way, the resolution at the difference frequency is constant. This is different from the approaches that shape pump

and Stokes beams where vibrational frequencies are targeted by shaping for the differences in the pump and Stokes; there, a high vibrational frequency requires large spectral features in the phase profile (for example, a sinusoid of only a few periods over the full pump spectrum). This approach therefore has a low spectral resolution in the high vibrational frequency range.

Furthermore, the broad bandwidth of the probe yields a way to interfere signals from different vibrational states in the output spectrum thereby enhancing the overall signal and suppressing the non-resonant contribution. As such, our approach is similar to the multi-probe approach in [20], except that it does not require distributing the energy over the pump and probe to create the multi-probe effect. Furthermore our method works on the full, spectrally-integrated response rather than a selected spectral region. Also the  $\pi$ -phase step introduced in the probe profile to reject non-resonant contributions as in [16, 18, 20] is not required here; the phase step in the resonant molecular response itself can be addressed. A further step in the probe profile is present in our scheme as well (as we use the same pulse for pump and probe) but is not required for the spectroscopy.

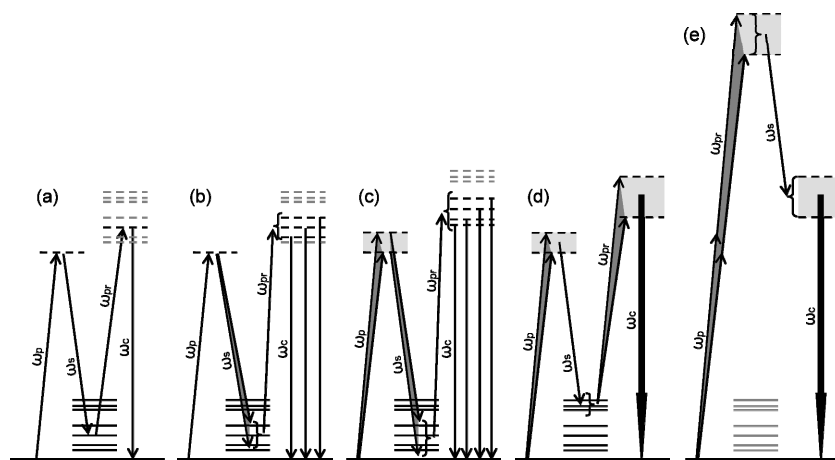


Fig. 1. CARS energy schemes a) Narrowband CARS, b) Multiplex CARS, c) Pump and Stokes broad, d) Pump and probe broad, e) Non-resonant energy scheme.

In this paper we demonstrate how new spectral phase shaping strategies can amplify the resonant features in the spectrum to such an extent that spectroscopy and microscopy can be done at high resolution, on the integrated spectral response without the need for a spectrograph. We identify line positions, widths, and relative intensities. This technique allows for spectroscopy at the resolution of the spectral phase shaper ( $0.5 \text{ cm}^{-1}$ ). We investigate here the spectral region around  $3000 \text{ cm}^{-1}$ . In this region strong and well separated O-H, C-H, and N-H lines are located, which facilitates the demonstration of the technique. Our Stokes pulse is centered at  $9396 \text{ cm}^{-1}$  ( $1064 \text{ nm}$ ,  $281.7 \text{ THz}$ ) with a temporal intensity FWHM of  $15 \text{ ps}$  ( $1 \text{ cm}^{-1}$ ). For the pump pulse and probe pulse (identical) we use a broadband Ti:Sapphire pulse around  $12500 \text{ cm}^{-1}$  ( $800 \text{ nm}$ ,  $375 \text{ THz}$ ) with a temporal intensity FWHM of  $60 \text{ fs}$  ( $230 \text{ cm}^{-1}$ ).

We start with a short description of the setup, which is followed by a number of simulations for a single transition to explain how we determine the vibrational frequency and line width. The relative cross sections (relative to the non-resonant background) in a multi-line spectrum can be determined by fitting. Measurements on acetone are compared to the simulations and literature. The paper concludes with an outlook on applications.

## 2. Setup

A schematic figure of the setup is presented in Fig. 2.

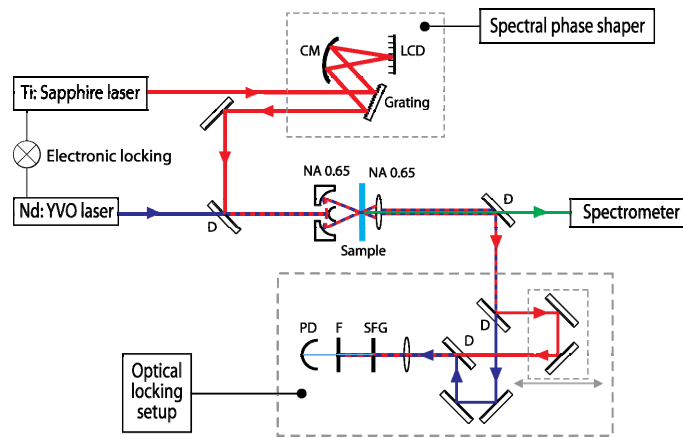


Fig. 2. Layout. CM (curved mirror), LCD (liquid crystal device), D (dichroic), F (short pass filter), PD (photodiode), and SFG (sum frequency generating crystal).

We use a tunable Ti:Sapphire oscillator from KM-Labs with a spectral FWHM of  $280\text{ cm}^{-1}$  centered around  $12267\text{ cm}^{-1}$  (815 nm, 368 THz). The energy per pulse is 2.8 nJ (repetition rate of 80 MHz). The liquid crystal device (LCD) of the spectral phase shaper has 4096 pixels with a pixel size of  $1\text{ }\mu\text{m}$  by  $6\text{ mm}$  with a pitch of  $1.8\text{ }\mu\text{m}$  (Boulder Nonlinear Systems). Usually spectral phase shaping techniques suffer from pixelation effects; in our case these are negligible because of an intentional increase in the crosstalk between pixels, which decreases the effective resolution. Effectively the spectral phase shaper has  $\sim 600$  degrees of freedom. For the absolute positioning of phase profiles the complete number of pixels can be used, which implies a positioning precision of  $0.47\text{ cm}^{-1}$  (14 GHz). Further details and description of the calibration of the spectral shaper setup can be found in an earlier publication [21]. The pulses of the Ti:Sapphire laser are pre-compressed by an external prism compressor (this prevents wasting degrees of freedom on the shaper to compensate simple dispersion) and shaped to be Fourier limited (at the position of the sample) by the spectral phase shaper using an evolutionary learning algorithm [22], with SHG signal from a thin ( $10\text{ }\mu\text{m}$ )  $\text{BiB}_3\text{O}_6$  crystal at the location of the sample as feedback. The desired spectral phase functions for the experiments as well as the higher order dispersion correction are applied by the spectral phase shaper.

The shaped Ti:Sapphire pulses are used as the pump and probe pulses in the CARS process. The Stokes pulse is generated by a 15 ps ( $1\text{ cm}^{-1}$ ) Nd:YVO laser ( $9396\text{ cm}^{-1}$  (1064.3 nm, 281.7 THz), Spectra Physics Vanguard). The laser systems are synchronized in a two-step locking system. The first step is based on the signals of two fast photodiodes; when this locking is achieved the second step is switched on, which is based on sum frequency generation (SFG) signal, where the Ti:Sapphire pulse is delayed 7 - 8 ps to coincide with the flank of the Nd:YVO pulse [23]. Two piezoelectric devices in the Ti:Sapphire laser cavity are controlled by feedback from the fast photodiodes or the SFG signal. The residual integrated jitter of the second stage of the locking system is 60 fs rms for a bandwidth of 100 Hz.

A reflective objective of 0.65 NA is used for focusing, without the addition of dispersion or chromatic aberration. The loss of light from low angles is acceptable since it is a minor contribution to the signal due to momentum conservation restrictions. The collection objective is a 0.65 NA regular glass objective. For the collection, low angles are important whereas dispersion is not. The collected light is sent to a spectrometer with a resolution of 0.25 nm and detected on a CCD array.

### 3. Simulating the CARS signal

We begin by describing the theoretical foundations of our approach, and demonstrate two ways, based on simple phase profiles, to extract the frequencies of vibrational resonances. Next we present means of finding the (effective) line widths, and the relative cross sections.

The total CARS signal has two major contributions as indicated in Fig. 1: a resonant and a non-resonant part. The resonant part originates from vibrational resonances and has the generic form shown in Eq. (1) [24]:

$$\chi_R^{(3)}(\omega) = \sum_R \frac{A_R}{\omega_R^2 - \omega^2 + 2i\omega\gamma_R}, \quad (1)$$

where  $A_R$ ,  $\omega_R$  and  $\gamma_R$  are the amplitude, frequency and line width of the vibrational resonances. The CARS spectrum can be expressed as:

$$I_{CARS}(\omega_c) \propto (P(\omega + \omega_s) \exp[i\Phi(\omega + \omega_s)]) \cdot (\chi_R^{(3)}(\omega) + \chi_{NR}^{(3)}) \otimes Pr(\omega) \exp[i\Phi(\omega)]^2 \quad (2)$$

where  $P(\omega)$  and  $Pr(\omega)$  are the intensity profiles of the pump and probe pulses. The spectral phase shaping is indicated by the phase function ( $\Phi(\omega)$ ). The Stokes pulse is spectrally narrow and unshaped, therefore we take only its frequency into account.  $\chi_{NR}^{(3)}$  is the non-resonant third-order susceptibility and is assumed to be constant (flat spectral response).

We analyze the simplest case of one transition in the center of the broad pump (- Stokes) pulse. The shaped pump and probe pulses are defined to have a FWHM of 7 THz ( $233 \text{ cm}^{-1}$ ), centered at 372 THz ( $12400 \text{ cm}^{-1}$ , 806.5 nm). The FWHM of the vibrational band is chosen to be 300 GHz ( $10 \text{ cm}^{-1}$ ). A positive  $\pi$ -step, located spectrally so that it compensates the phase of the vibrational resonance, is applied to the pump pulse. Since the probe is also shaped, the CARS spectrum shows a dip in the center due to destructive interference of the additional phase step. The normalized components of the laser pulse are shown in Fig. 3(a); the normalized intensity and phase profile of the vibrational resonance are shown in Fig. 3(b). Figures 3(c) and 3(d) show the resulting resonant and non-resonant CARS spectra. The black lines represent the calculated spectra for the shaped pulse (Fig. 3(a)). The thin red (Gaussian) lines are for comparison and indicate the unshaped (flat phase) spectra. Here, the intensity reflects the chosen values for  $\chi_R^{(3)}$  and  $\chi_{NR}^{(3)}$ , 1 and 10 respectively. Note that the intensity of the vibrational band scales quadratically with the value of  $\chi_R^{(3)}$ .

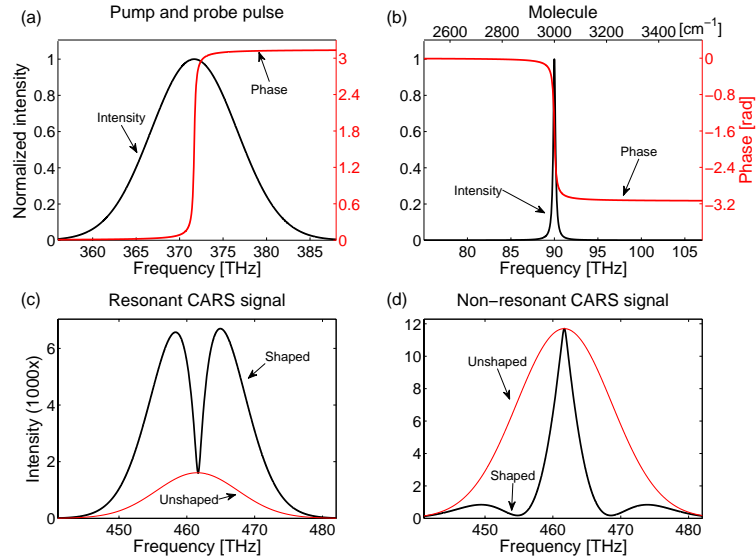


Fig. 3. (a). Spectral intensity and phase profile of the pump and probe pulse. (b). Intensity and phase of a vibrational resonance. (c) and (d). The resonant and non-resonant CARS contribution for the spectral phase in (a) (black) and for a flat spectral phase (thin red).

Figure 4 shows a simulation where the positive phase step, shown at the center of the band in Fig. 3, is now swept through the spectrum. The horizontal axis provides the location of the phase step, and the vertical axis shows the integrated CARS signal, normalized to the total CARS signal for a flat spectral phase. When the compensating (positive) phase step is swept through the spectrum, a maximum of the integrated resonant CARS signal occurs when the phase step coincides with the resonance, despite the local spectral dip (Fig. 3(c)). The integrated *non*-resonant CARS signal is lowest when the phase step is in the center of the spectrum, and highest when the phase step is outside the laser spectrum. Hence, this sweeping method reveals resonances as local maxima that coincide with the position of the phase step. As a caveat, we note that closely spaced resonances reduce each others visibility and transitions with a low cross section are easily lost in a dominant non-resonant background. Furthermore, our simulations show that when weak resonances are in the vicinity of the main vibration band, the peak in the integrated signal will be slightly shifted. For a sharp phase step, the width of the peak in the center corresponds to the width of the resonance.

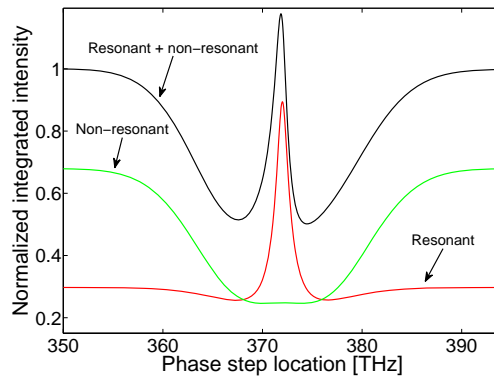


Fig. 4. Integrated CARS signal for a negative Lorentzian phase profile (positive phase step).

From the spectrally resolved signals the positive phase step creates a dip in the resonant CARS-spectrum, whereas the non-resonant signal shows a maximum at the same spectral position (Figs. 3(c), 3(d)). For a *negative* phase step, the non-resonant CARS-spectrum will be the same, because the non-resonant CARS-spectrum is independent of the sign of the phase. However, interference in the resonant CARS-spectrum will cause an enhancement at that frequency due to the constructive interference of an effective  $2\pi$ -phase step. The negative phase step yields a negligible effect on the integrated signal, in comparison with the positive phase step, but produces sharp spectral features that are easily identified in a spectrally resolved measurement. Figure 5 shows the effect of such a negative phase step when the resonance and phase step are located in the center of the pump (- Stokes) spectrum.

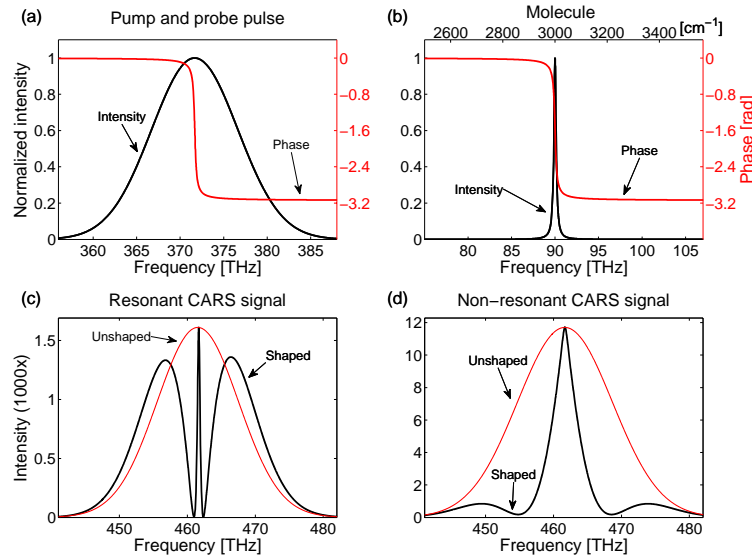


Fig. 5. (a). Spectral intensity and phase profile of the pump and probe pulse. (b). Intensity and phase of a vibrational resonance. (c). and (d). The resonant and non-resonant CARS contribution for the spectral phase in (a) (black) and for 0 flat spectral phase (thin red).

Note that a sharp feature is created in the resonant as well as in the non-resonant spectrum. These features coincide in the CARS spectrum only when the phase step is at the precise location of the vibrational band. For other positions of the phase step, the features appear at different positions in the CARS spectrum. A measured CARS spectrum always contains both a resonant and non-resonant contribution, whose interference influences the position of the feature in the integrated spectrum. Figure 6 shows contour plots of phase step sweeps with (a) positive phase step, (b) negative phase step and (c) the difference, where the horizontal axes represent the location of the phase step and the CARS-spectra are displayed along the vertical axes. Since the non-resonant contribution is independent of the sign of the phase profiles, the difference contains only the resonant features. Note that resonant contributions from the flat parts of the phase profiles are also eliminated. However, the non-resonant contribution is still present as an overall gain factor. Since it is present in the spectral intensity through the mixing term between the resonant and non-resonant contributions, (sometimes referred to as the homodyne amplification [7]), it is also present in the difference plot and due to the phase asymmetry it results in an asymmetry in the difference plot.

To understand the CARS spectrum for any position of the phase step we outline the contributions according to Eq. (2). The first part, the convolution of the pump and Stokes pulses, shifts the pump profile to the difference frequency without changing the phase profile. The multiplication with the resonance response can be regarded as a sampling of this shifted pump profile by the resonances of the molecule. Since the resonances have fixed positions

they always sample the same part of the pump profile. At this point the treatment has to be split into two distinctly different scenarios that are responsible for distinct features in the 2D spectra.

The first scenario is for a  $\pi$ -phase step that does *not* coincide with a resonance so that the result of the sampling of the shaped pump by the molecular response is just a copy of the molecular resonance response where a constant phase (0 or  $-\pi$ ) is added to the narrow phase profile of the resonance (i.e. a negative phase step). The amplitude of the response is multiplied by the amplitude of the corresponding part of the pump spectrum. For the final part of Eq. (2), the shaped probe has to be convoluted with the narrow sample. This convolution can be approximated as the creation of two copies of the (shaped) probe spectrum with opposite phase, separated by a distance equal to the width of the resonance (rather like a differentiator). The result of this combination is an almost complete cancellation of the spectrum except in the vicinity of sharp transitions (such as the shaped  $\pi$ -step) where a sharp feature is created. When the phase step scans through the profile, the sharp feature scans with the step, creating a distinct feature with a slope of 1 in Fig. 6.

The second scenario is when the applied  $\pi$ -phase step overlaps with (and cancels) the molecular phase step. In this scenario the sampling results in a copy of the amplitude of the molecular response except that it now has a flat phase. In the final convolution step with the probe spectrum therefore, the full (shaped) probe spectrum is transferred to the final spectrum. This full transfer creates a vertical features in Figs. 6(a)-6(c) and an integrated effect in the Fig. 4 and Fig. 8. Note that multiple separated resonances will cause multiple features with slope 1 as well as multiple vertical features.

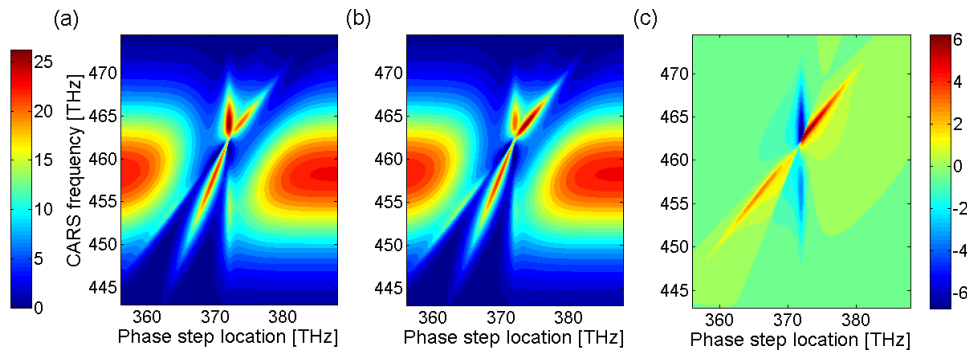


Fig. 6. (a) and (b) CARS-spectra contour plots for a sweep with a positive (a) and negative (b) phase step. c) The difference between a negative and a positive phase step sweep.

The non-resonant part of the CARS signal is the convolution of the pump (- Stokes) and probe without the intermediate sampling. The spectral region around the phase shift acts as a local differentiator that samples the phase shift in the probe and creates a feature in the output. When the phase step is swept through the spectrum, the feature (the combination of a moving differentiator sampling a moving phase step) moves at twice the speed of the sweep and shows up as a feature of slope 2 in Figs. 6(a) and 6(b). The broad signals on the left and right in Figs. 6(a) and 6(b) are mostly due to the non-resonant contribution and partly due to the resonant signal from the flat (phase) wings of the resonance. The different features cross at the resonance frequency (- Stokes). The vertical features in Fig. 6(b) are less pronounced because the phase of the resonance is not completely cancelled by the negative phase step over the full width of the resonance. The projection on the molecule (sampling) therefore does not produce a flat phase.

The line width of one single resonance (or the effective line width for multiple closely spaced resonances) can be found by varying the 'slope' or width of the phase step, while keeping the step centered on the transition. Here we define the profile for a certain width ( $2\gamma$ )

of the step as the phase profile that corresponds to a Lorentzian profile with the same FWHM ( $2\gamma$ ) of the intensity:

$$\phi(\omega, \gamma) = \arg \left[ \sqrt{\frac{\gamma}{\pi}} \frac{1}{(\omega + i\gamma)} \right] \quad (3)$$

With this definition of the width, the width of the step corresponds to the width of a (vibrational) transition in a natural way

When the width of a positive phase step matches with the width of the vibrational resonance, the integrated resonant signal is maximized. Unfortunately, as the width of the phase step increases the non-resonant contribution also increases. Again the resonant features are revealed by subtracting the results for a positive phase step with the results of a negative phase step. Figure 7 shows the integrated CARS signal for a positive phase step, a negative phase step, and the difference. The horizontal axis represents the width of the phase step in  $\text{cm}^{-1}$ . On the vertical axis the integrated signal is given, normalized to the signal for a flat phase profile. The simulated vibrational resonance has a FWHM of  $50 \text{ cm}^{-1}$  (1.5 THz).

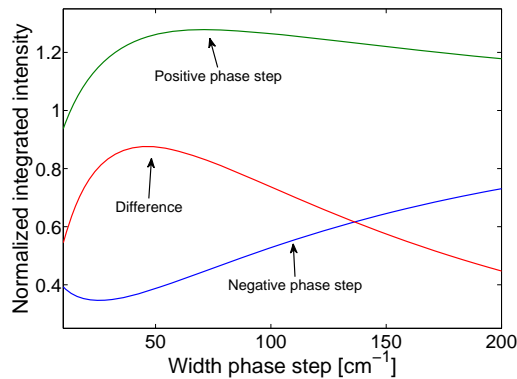


Fig. 7. Integrated CARS signals as a function of the width of the phase profile. Green line: positive phase step. Blue line: negative phase step. Red line: the difference, for which the maximum indicates the line width of the resonance

As can be seen in Fig. 7, the maximum of the difference signal does not yield directly the FWHM of the simulated vibrational resonance. The maximum also depends on the spectrum of the pump and probe pulses. But, since this spectrum is known, the width can be extracted by fitting. The maximum is independent of the cross section; the cross section will only influence the height of the difference.

Hence, by the previous described methods the vibrational frequencies and line widths can be obtained. In addition the relative cross sections can be found by fitting the measurements to the theory, keeping the obtained frequencies and line width fixed, and varying the cross section as a free parameter.

#### 4. Measurements and discussion

We now present experimental measurements that demonstrate the enhancement of the resonant part of the integrated CARS signal by use of a compensating (positive) phase step. We do this in acetone, which has one strong resonance at  $2923 \text{ cm}^{-1}$  as well as several neighboring weak resonances [25]. Figure 8 shows the experimental result for spectrally sweeping a positive phase step, with a width of  $5 \text{ cm}^{-1}$  (0.15 THz), through the pump and probe spectrum. The width of this phase step is a factor of four below the expected bandwidth of the main vibration. The horizontal axis provides the location of the phase step, and the vertical axis shows the integrated CARS signal normalized to the total CARS signal for a flat spectral phase. The pump and probe pulses are identical with a center frequency of  $12267 \text{ cm}^{-1}$  (368 THz) and an intensity FWHM of  $277 \text{ cm}^{-1}$  (8.3 THz). The Stokes pulse has a center

frequency of  $9396\text{ cm}^{-1}$  (282 THz) and an intensity FWHM of  $1\text{ cm}^{-1}$  (30 GHz). The acetone (Merck, purity > 99.5%) sample is sandwiched between a cover glass of thickness  $\sim 0.1\text{ mm}$  and a 1 mm thick microscope slide. Paraffin wax is used as spacer.

Figure 8 shows one strong resonance for a phase step at 369.82 THz, corresponding to a resonance frequency of  $2940\text{ cm}^{-1}$ , slightly higher than the expected Raman frequency of  $2923\text{ cm}^{-1}$  [25]. The shift can be explained by interference effects from the smaller vibrational resonances within a window of  $100\text{ cm}^{-1}$  (3 THz). This example shows that the method works for strong isolated resonances, and gives an indication of the line width when a very steep phase profile is used. The simulation is calculated using one vibrational resonance where the line width and the cross section (compared to the non-resonant background) are varied. The fit parameters are  $26\text{ cm}^{-1}$  for the line width and 25 for  $\chi_R^{(3)} / \chi_{NR}^{(3)}$  (amplitude).

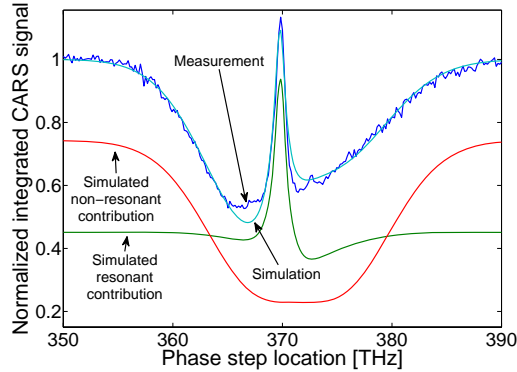


Fig. 8. Normalized integrated CARS signal for acetone, with a positive phase step swept through the spectrum of the pump and probe pulses.

Figure 9 shows contour plots of measured spectra for a positive phase step sweep (a), a negative phase step sweep (b), the difference (c), and the integrated CARS signals (d). The horizontal axes in all plots of Fig. 9 represent the location of the phase step, and the vertical axes show the CARS spectra (a-c) or the integrated CARS signal (d). The phase steps have a width of  $1\text{ cm}^{-1}$ . From the 2D plots, the main peak is now determined from the crossing point of the non-resonant feature (slope 2) and the resonant feature (slope 1) and is found to be  $2923\text{ cm}^{-1}$  matching the value from literature [25]. The other lines remain hidden in the noise in Fig. 9(c).

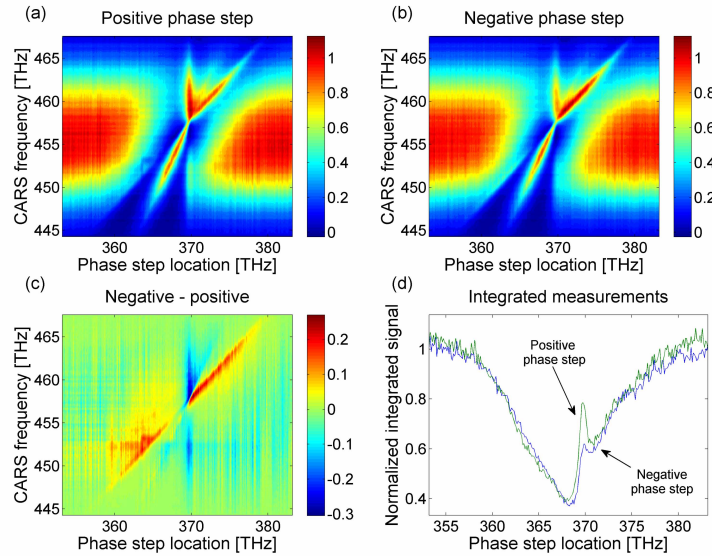


Fig. 9. Results for acetone a) Contour plot for a negative phase step. b) Contour plot for a positive phase step. c) Contour plot for the difference. d) Integrated spectra for the negative and positive phase step.

As shown in the previous section, the line width for a single resonance can be examined by tweaking the width of the phase step at the vibrational band and comparing the integrated CARS spectra. However a real molecule has many resonances, even in the case of acetone the weak resonances near the strong resonance influence the experiment. This influence is shown in Fig. 10. Figure 10(a) shows the data with a fit using only one vibrational resonance. Figure 10(b) shows the data where all five resonances in vicinity are taken into account. On the horizontal axis the width of the phase step is plotted and the vertical axis shows the integrated CARS signals, normalized to a flat phase profile.

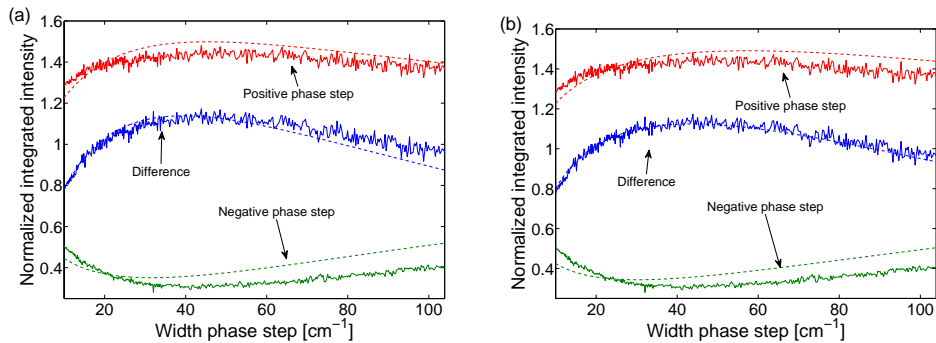


Fig. 10. Effective line width estimation of acetone. a) Fitted for one transition. b) Fitted for five transitions.

The simulated lines in Fig. 10(a) are for a vibrational resonance at  $2936\text{ cm}^{-1}$ , 10 for  $\chi_R^{(3)}/\chi_{NR}^{(3)}$  (amplitude), and a line width of  $38\text{ cm}^{-1}$ . This line width is much broader than determined from the measurement shown in Fig. 8 ( $23 \pm 2\text{ cm}^{-1}$ ). We attribute this difference to the smaller resonances near the main resonance. Thus Fig. 10(a) yields an effective line width and effective line amplitude. Figure 10(b) shows the result when 5 lines are used with vibrational frequencies taken from literature ( $2698\text{ cm}^{-1}$ ,  $2850\text{ cm}^{-1}$ ,  $2923\text{ cm}^{-1}$ ,  $2966\text{ cm}^{-1}$ , and  $3004\text{ cm}^{-1}$  [25]), free line amplitudes (8, 1, 27, 12, 12 for  $\chi_R^{(3)}/\chi_{NR}^{(3)}$ ) and free line widths

(17 cm<sup>-1</sup>, 22 cm<sup>-1</sup>, 16 cm<sup>-1</sup>, 26 cm<sup>-1</sup>, 11 cm<sup>-1</sup>). Fitting the measurements with five resonances improves the simulated difference line in comparison to the fit to one line.

## 5. Conclusions and outlook

We have demonstrated a new spectral phase shaping strategy for CARS spectroscopy. Vibrational transitions can be identified with a resolution limited by the resolution of the shaper (here, 0.5 cm<sup>-1</sup>). Furthermore we have introduced a method for measuring the width for isolated spectral lines and an effective line width for a combination of lines. Relative cross sections can be extracted from the spectral sweep data. We have also shown the possibility to disentangle the resonant and non-resonant contribution of the total CARS signal.

Using spectral phase shaping we are planning to create molecule-specific pulses where the selectivity is based on multiple transitions. Label-free investigation of a sample based on multi line profiles increases the specificity. As long as the resonances have a discernable phase character, a richly structured spectrum will increase the chemical contrast. Imaging with increased selectivity and rejected background will be the aim of further research. By lowering the difference frequency between the pump and Stokes pulses the fingerprint (~100-1100 cm<sup>-1</sup>) region can be accessed.

## Acknowledgments

The authors are grateful to R. J. Moerland for useful suggestions and F. B. Segerink for practical issues. This work is part of a research project of the 'Stichting voor Fundamenteel Onderzoek der Materie (FOM)', which is financially supported by the 'Nederlandse Organisatie voor Wetenschappelijk Onderzoek (NWO)'.